Theoretical investigation of molecular and electronic structure changes of the molecular magnet Mn_{12} cluster upon super-reduction

Yoshio Nishimoto[1], Hirofumi Yoshikawa[1], Kunio Awaga[1], Marcus Lundberg[*,2], and Stephan Irle[**,1,3]

[1] Department of Chemistry & Research Center for Materials Science, Nagoya University, Nagoya, 464-8602, Japan

[2] Department of Chemistry – Ångström Laboratory, Uppsala University, SE-751 20 Uppsala, Sweden

[3] Institute of Transformative Bio-Molecules (WPI-ITbM), Nagoya University, Nagoya, 464-8602, Japan

Abstract. Density functional theory calculations on the neutral $[Mn_{12}]^0$ molecular magnet and super-reduced $[Mn_{12}]^{8-}$ cluster were employed to investigate the experimental geometrical changes observed during discharging in a molecular cluster battery. It was found that for relevant low-spin states the eight electrons added in $[Mn_{12}]^{8-}$ are mainly added to the outer eight Mn atoms, causing elongation of the bonds between outer Mn and their surrounding O atoms, while the inner Mn_4 cluster is less affected by the reduction.

* Corresponding author: e-mail marcus.lundberg@kemi.uu.se, Phone: +46 18 471 3708, Fax: +46 18 471 3633

** Corresponding author: e-mail sirle@chem.nagoya-u.ac.jp, Phone/Fax: +81 52 747 6397

1 Introduction

The molecular cluster, $[Mn_{12}O_{12}(CH_3COO)_{16}(H_2O)_4]$ (abbreviated as Mn_{12}, see Figure 1), is famously known as a single molecular magnet. The cluster was first synthesized by Lis in 1980 [1], and has been investigated experimentally [2-5] and theoretically [3,6] ever since because of its intriguing properties. Regarding the spin state of the neutral cluster, it was experimentally shown that the cluster has a total spin of S = 10 [2]. However, the intriguing property of the Mn_{12} cluster is not only the spin property: experimentalists recently found that the Mn_{12} cluster exhibits a high discharging capacity of more than 200 Ah/kg [4], which is even higher than that of ordinary Li-ion batteries (about 150 Ah/kg) [7,8]. Moreover, they found in the experimental capacity and X-ray absorption fine structure (XAFS) analysis that the Mn_{12} cluster exhibits a super-reduced state accepting 8 surplus electrons during discharging, and an even higher total spin, S = 14 [5]. A Mn *K*-edge extended XAFS (EXAFS) study [4] also suggested that Mn-O distances significantly elongate from 1.9 Å to 2.2 Å during super-reduction.

In spite of these interesting properties and several theoretical investigations of the neutral Mn_{12} system, there is just one report [6] which involves multi-step reduction of the Mn_{12} cluster. In Ref. [6], Park *et al*. investigated reduced states up to $[Mn_{12}]^{4-}$, mainly discussing magnetic properties but not structural changes. In this work, we performed structural and spin state analysis of the neutral ($[Mn_{12}]^{0}$) and the super-reduced ($[Mn_{12}]^{-8}$) electronic states.

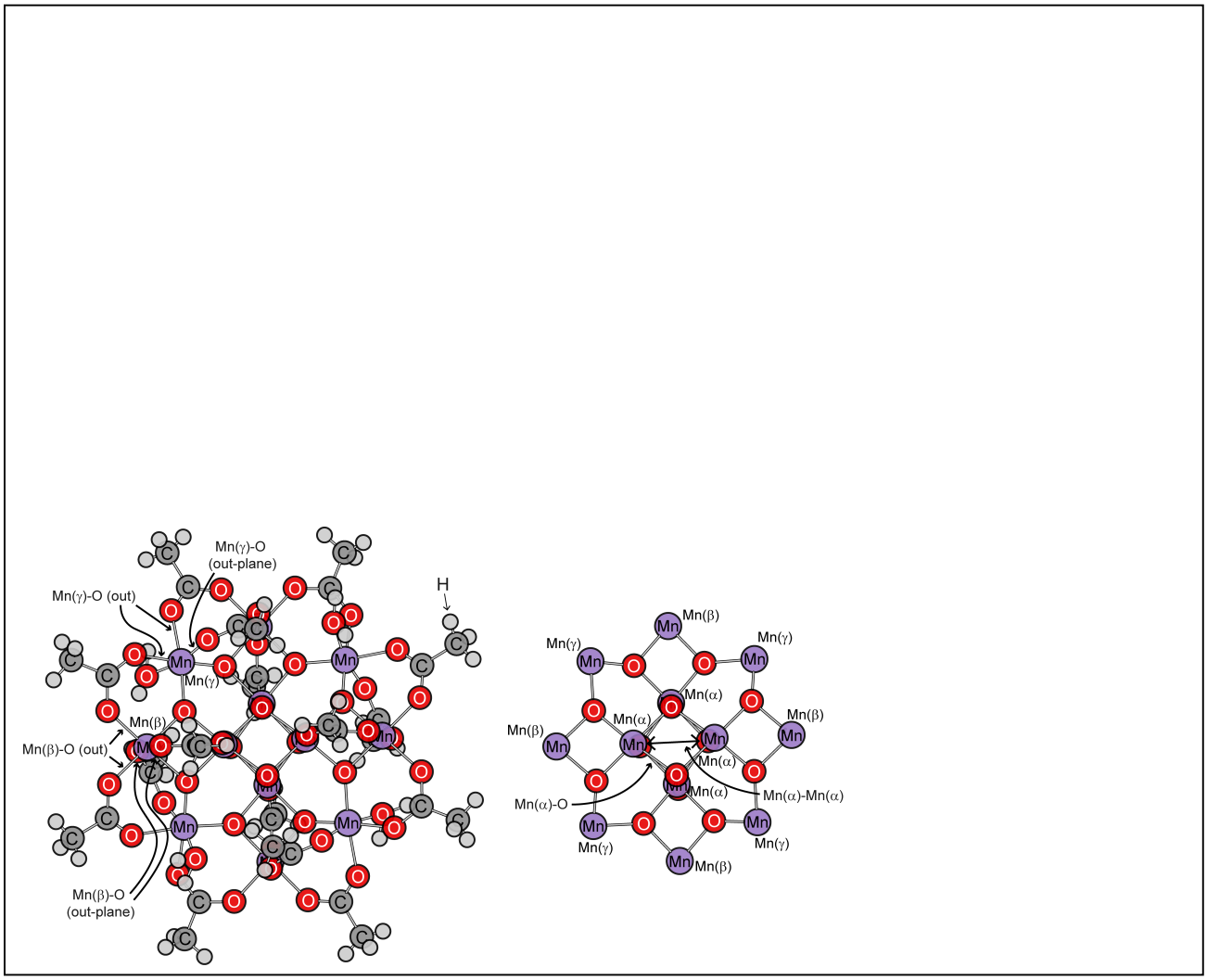

Figure1. Left: Structure of [Mn_{12}] ($Mn_{12}C_{32}O_{48}H_{56}$) cluster, taken from an X-ray study, with hydrogen atoms optimized at the RI-BP86/SV(P) level of theory. Right: $Mn_{12}O_{12}$ core cluster where 16 CH_3COO and 4 H_2O are abbreviated, and the symbols (a, b, g) next to Mn atoms specify which group they belong to.

2 Computational Methodology

All electronic structure calculations and first principles molecular dynamics (FPMD) simulations were carried out within the density functional theory (DFT) [9,10] framework, as implemented in TURBOMOLE [11] version 6.3. We first performed calculations for the neutral cluster with BP86 [12,13], TPSSh [14], B3LYP [15] (with VWN(V) correlation) and BHLYP [16] functionals to compare DFT structures with X-ray data [1].

For BP86 calculations, the resolution of the identity (RI) approximation [17] was adopted to save computational cost. In all calculations, we employed the def-SV(P) basis set [18] [abbreviated as SV(P)] and the corresponding auxiliary basis set [19] for the RI approximation. We employed spin-unrestricted Kohn-Sham orbitals and energies without broken-symmetry corrections throughout this work. No symmetry constraints were applied. In the molecular cluster battery (MCB) experiment [4,5], the cathode was made of conductive carbon and the Mn_{12} cluster, and the electrolyte was a mixture of diethyl carbonate and ethylene carbonate. Due to computational limits, we cannot explicitly include such an environment in our DFT calculations, therefore we simply used the conductor-like screening model (COSMO) [20] to take into account the effect of environment and for stabilizing excess electrons. A high dielectric constant of 100.0 was used for this purpose. Natural population analysis [21] was performed to evaluate the obtained electronic structure.

The initial geometry was taken from the X-ray data [1] of the neutral cluster, which lacks the coordinates of hydrogen atoms. Therefore, we first optimized the position of the missing hydrogen atoms at the RI-BP86/SV(P) level of theory while all other atoms were fixed. Then, separate geometry optimizations were performed for all spin states.

We additionally performed an RI-BP86/SV(P)-based FPMD simulation of the super-reduced cluster to consider finite-temperature effects. The environmental temperature was set to 298.15 Kelvin and it was kept constant using the Nose-Hoover thermostat [22-24]. The time step was 0.968 femtosecond (40 a.u.), and 1,000 time integration steps were performed using the Leapfrog Verlet algorithm. The total simulation covers therefore roughly one picosecond.

3 Results and Discussion

3.1 Neutral cluster We first briefly discuss the spin density and structural parameters of $[Mn_{12}]^0$, in comparison to the X-ray structure [1]. We considered 15 different spin states from $S = 0$ to $S = 22$, and performed geometry optimizations for each state (Table S1; Figure and Table numbers preceded by an "S" refer to material given in the Supporting Information). Relative energies indicate that the low-spin (LS) state (LS1, Entry 14), where each inner Mn atom (Mn(a)) has three beta electrons, and each outer

Mn atom (Mn(b) and Mn(g)) has four alpha electrons (S = 10), affords the lowest energy minimum in agreement with previous theoretical calculations [6]. In this solution, there is antiferromagnetic coupling between the di-μ-oxo,μ-carboxy bridged Mn(a)-Mn(b) atoms, while all other pairs of Mn atoms have longer distances and are ferromagnetically coupled. However, the second-lowest spin state with S = 2 (Entry 6) is very close with only ~1 kcal/mol separation. The predicted oxidation state of both solutions, deduced from the spin density on Mn centers, is formally Mn_4(IV)Mn_8(III). The corresponding high-spin (HS) solution (HS1), where all b-spins on Mn(a) are flipped to a-spin, has S = 22 (Entry 15) and is highest in relative energy. Its oxidation state is practically the same as that of the LS1 solution. According to our calculation, the LS1 solution is more stable than the corresponding HS1 solution by 14.01 (RI-BP86), 9.87 (TPSSh), 5.53 (B3LYP) and 3.01 (BHLYP) kcal/mol. This trend reflects the different contributions of exact exchange in the density functionals. The exchange interaction is overestimated in the Hartree-Fock theory, which results in the over-stabilization of the HS1 state over the LS1 state. In any case, the relatively small energy differences show that the spin coupling between different manganese sites is relatively weak.

Table 1 shows the structural parameters and natural spin densities at the RI-BP86/SV(P) level of theory along with the experimental X-ray geometry as reference. The corresponding data for other functionals is presented in Table S2. The RI-BP86 calculation agrees sufficiently well with the X-ray structure, since bond lengths show maximum deviations of 0.05 Å. For the sake of computational limits, we therefore decided to use the BP86 functional with RI approximation in the following subsections.

Table 1 Structural parameters (Å) and natural spin densities for the $[Mn_{12}]^0$ cluster at the RI-BP86/SV(P) level of theory. See Figure 1 for the definition of the structural parameters. The root mean square deviation (RMSD) is computed between the X-ray and the optimized Cartesian coordinates, excluding hydrogen atoms.

Structural parameters

	X-ray	RI-BP86	
		HS1	LS1

Mn(a)-Mn(a)	2.86	2.91	2.90
Mn(a)-O	1.91	1.94	1.93
Mn(b)-O (out-plane)	2.23	2.19	2.20
Mn(b)-O (out)	1.94	1.98	1.97
Mn(g)-O (out-plane)	2.11	2.07	2.10
Mn(g)-O (out)	1.98	2.04	2.01
RMSD		0.17	0.14

Natural spin density

	HS1	LS1
Mn(a)	2.96	-2.55
Mn(b)	3.72	3.65
Mn(g)	3.72	3.60

3.2 Super-reduced cluster Our aim in this letter is to correlate the geometrical change observed during the experimental super-reduction [4,5] with a corresponding change in the electronic state. Starting with the optimized structures at the selected spin states with lower energies (Entries 5, 6, 12, 14) and HS1 (Entry 15), we added 8 electrons in three ways, (8 a, 0 b), (0 a, 8 b) and (4 a, 4 b) electrons, and optimized the molecular geometries for a total of 15 different spin states. The energies of the optimized structures can be found in Table S3. According to our calculations, the most stable electronic structures derives formally from the HS1 state of the neutral cluster after spin flip, and corresponds to reduction of both inner Mn(a) (around one excess electron) and outer Mn(b,g) (around seven excess electrons), with $S = 18$ (Entry 15-8b in Table S3).

However, the experiment [5] implies that the spin quantum number of $[Mn_{12}]^{8-}$ is $S = 14$ (Entry 14-8a in Table S3). In broken-symmetry DFT, the $S = 14$ state is formally $Mn_4(IV)Mn_8(II)$, with the spin on the inner Mn(a) antiferromagnetically coupled to the outer Mn. To the contrary, our calculation suggests that this state is unstable by 30.92

kcal/mol, compared to the previously mentioned lowest calculated energy state with S = 18. One possible reason for the disagreement with experiment is that the experimental spin state (S = 14) cannot be described by the single-determinant wave function used in DFT. To compute this state accurately, we need to perform a multi-reference calculation, which is far beyond the current computational capability. One possible reason for the discrepancy is that reduction of the inner Mn(a) would require electron transfer through the outer Mn: However, this process is slow due to the antiferromagnetic coupling between inner and outer Mn in the $[Mn_{12}]^0$ state [25]. The low-energy spin states, e.g., the S = 18 state could then lie on a decomposing pathway of $[Mn_{12}]^{8-}$, as the degradation of the battery performance has been observed in the experiment [4,5]. Another reason could be that lithium counterions, present in the MCB setup, play an important role for the stabilization of the experimentally determined S = 14 state.

Increasing the amount of HF exchange increases the HOMO-LUMO gap and favors localization of the electron density, similar to the effect of on-site Coulomb repulsion in Ref. [26]. However, LS3 remains more stable than LS2 for all tested functionals, see the Supporting Information. For the simplicity of discussion, in the following section we will focus only on the LS2 (S = 14) and LS3 (S = 18) states (Entry 14-8a and 15-8b in Table S3), as the former is predicted by experiment [5] and the latter is predicted by our theoretical calculations.

Table 2 Structural parameters (Å) and natural spin densities for the $[Mn_{12}]^{8-}$ cluster at the RI-BP86/SV(P) level of theory. See Figure 1 for the definition of the structural parameters.

Structural parameters

	LS2	LS3
Mn(a)-Mn(a)	2.88	2.89
Mn(a)-O	1.94	1.97
Mn(b)-O (out-plane)	2.40	2.39
Mn(b)-O (out)	2.19	2.12

Mn(g)-O (out-plane)	2.16	2.14
Mn(g)-O (out)	2.26	2.22

Natural spin density		
	LS2	LS3
Mn(a)	-2.31	*a*
Mn(b)	4.47	3.99 – 4.37
Mn(g)	4.43	4.41 – 4.50

[a] -3.49, -3.40, 2.76, 3.66

Characteristic geometrical parameters for $[Mn_{12}]^{8-}$ at both LS2 and LS3 states are shown in Table 2. We notice that the geometry of the inner cluster, which contains Mn(a), does not change significantly in both solutions. This can be easily understood considering that the inner Mn atoms do not take up more than one excess electron. On the other hand, Mn(b)-O (out-plane), Mn(b)-O (out), Mn(g)-O (out-plane) and Mn(g)-O (out) distances changes are relatively clear, especially Mn(b)-O (out-plane) changes by 0.20 Å (LS2) and 0.20 Å (LS3) and Mn(b)-O (out) also does by 0.22 Å (LS2) or 0.14 Å (LS3) after super-reduction. Our result well reproduces the bond elongation observed experimentally in Refs. [4] and [5], where the *in situ* Mn *K*-edge EXAFS spectrum suggests that the Mn-O bond distance increases during discharging. We estimated these bond lengths after reduction to be about 2.2 Å. According to our calculation, both LS2 and LS3 solutions reproduce this bond elongation to a similar extent, as the Mn(b)-O and Mn(g)-O bonds increase in length, and the change of the Mn atoms during reduction is practically the same: the oxidation state and the number of unpaired electrons on them change from Mn(III) to Mn(II) and from four to five in both cases, respectively.

The elongation of Mn-O distances can be reasonably explained by ligand field theory. The coordination of Mn(b) and Mn(g) is roughly octahedral, thus five *d* orbitals split into

triply-degenerate (t_2) and doubly-degenerate (e^*). Each Mn (b) and Mn(g) has four a-spin electrons at $[Mn_{12}]^0$, so additional electrons fill the remaining e^* orbital. Occupying the anti-bonding e^* orbital results in the elongation of the distance between Mn and ligands.

3.3 Molecular dynamics simulation for $[Mn_{12}]^{8-}$ Since the environmental temperature of the MCB discharging experiment is not 0 K, we performed an MD simulation to characterize how the structure of the super-reduced cluster is affected by a finite temperature. Consistent with the experimentally observed spin state, we selected the LS2 (S = 14) state of $[Mn_{12}]^{8-}$ in this FPMD simulation.

The distribution of bond distances derived by Gaussian broadening (s = 0.1) during the dynamics was plotted in Figure 2. If a distance $R_{A\text{-}B}$ between atoms A and B satisfies $R_A + R_B - 0.5 \le R_{A\text{-}B} \le R_A + R_B + 0.5$, where R_A and R_B are the covalent radii of elements, R_H = 0.31 Å, R_C = 0.67 Å, R_O = 0.66 Å and R_{Mn} = 1.61 Å [27], we assume that there is a bond between atoms A and B. All plots are normalized. The red solid line is the average of the distribution over 501st to 1,000th time steps of the FPMD simulation at $[Mn_{12}]^{8-}$, and the red dashed and blue dotted lines indicate the bond lengths of optimized geometries of $[Mn_{12}]^{8-}$ at LS2 and $[Mn_{12}]^0$ at LS1 solutions. The most prominent difference between blue dotted ($[Mn_{12}]^0$) and red solid and dashed ($[Mn_{12}]^{8-}$) lines can be found around 1.8 Å ~ 2.5 Å, where the blue line has a higher peak at 1.94 Å and the red line is relatively weak and becomes broad at that region. The region corresponds to Mn-O bond distance, thus the change comes from the elongation of Mn(b)-O and Mn(g)-O distances, and this is indeed the case in our simulation. As discussed in the previous subsection, we find in the geometry optimization that Mn(b)-O and Mn(g)-O bonds are elongated by about 0.2 Å. The elongation can be seen from the shift of the bond length distribution: the broad foot around 2.0 Å ~ 2.5 Å emerges at the cost of the weakening peak around 2.0 Å.

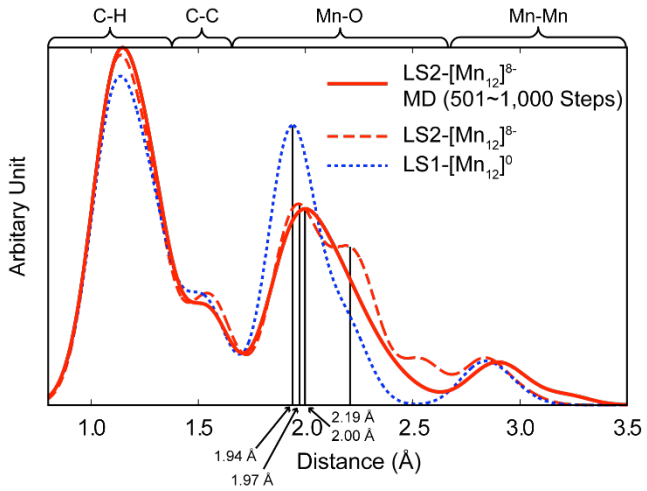

Figure 2 Distribution of bond lengths for $[Mn_{12}]^{8-}$ (average of 501st ~ 1,000th MD steps and optimized geometry) and $[Mn_{12}]^{0}$ (optimized geometry).

4 Conclusions

We performed density functional theory calculations for Mn_{12} cluster at neutral ($[Mn_{12}]^{0}$) and super-reduced ($[Mn_{12}]^{8-}$) states to clarify the changes observed in experiment [4,5]. For $[Mn_{12}]^{0}$, the lowest energy spin state we obtained agrees with the previous report by Park *et al*. [6], and we confirmed that the RI-BP86/SV(P) level of theory gave moderately reliable geometrical results for the cluster. Based on our calculations for $[Mn_{12}]^{8-}$, the elongation of Mn-O distance observed in experiment during super-reduction is predicted to come from the reduction of the outer Mn atoms, which causes the elongation of Mn(b)-O and Mn(g)-O distance, while the inner cluster involving Mn(a) atoms remains nearly unchanged. Molecular dynamics simulation at room temperature supports this observation.

Acknowledgements Computations were performed using the resource of Research Center for Computational Science, Okazaki, Japan. Y. N. is supported by Research Fellowships of the Japan Society for the Promotion of Science for Young Scientists. M. L. acknowledges financial support from the Marcus and Amalia Wallenberg foundation, the “Stig Hagström stipend”.

Supporting information Supplementary data associated with this article can be found, in the online version, at doi:

References

[1] T. Lis, Acta Cryst. B **36**, 2042 (1980).

[2] A. Caneschi, D. Gatteschi, and R. Sessoli, J. Am. Chem. Soc. **113**, 5873 (1991).

[3] D. Foguet-Albiol, T. A. O'Brien, W. Wernsdorfer, B. Moulton, M. J. Zaworotko, K. A. Abboud, and G. Christou, Angew. Chem. Int. Ed. **117**, 919 (2005).

[4] H. Wang, S. Hamanaka, T. Yokoyama, H. Yoshikawa, and K. Awaga, Chem. Asian J. **6**, 1074 (2011).

[5] H. Wang, Ph.D. thesis, Nagoya University, September 2011.

[6] K. Park and M. R. Pederson, Phys. Rev. B **70**, 054414 (2004).

[7] J.-M. Tarascon and M. Armand, Nature **414**, 359 (2001).

[8] M. Armand and J.-M. Tarascon, Nature **451**, 652 (2008).

[9] P. Hohenberg and W. Kohn, Phys. Rev. **136**, B864 (1964).

[10] W. Kohn and L. J. Sham, Phys. Rev. **140**, A1133 (1965).

[11] R. Ahlrichs, M. Bär, M. Häser, H. Horn, and C. Kölmel, Chem. Phys. Lett. **162**, 165 (1989).

[12] A. D. Becke, Phys. Rev. A **38**, 3098 (1988).

[13] J. P. Perdew, Phys. Rev. B **33**, 8822 (1986).

[14] J. M. Tao, J. P. Perdew, V. N. Straroverov, and G. E. Scuseria, Phys. Rev. Lett. **91**, 146401 (2003).

[15] A. D. Becke, J. Chem. Phys. **98**, 5648 (1993).

[16] A. D. Becke, J. Chem. Phys. **98**, 1372 (1993).

[17] C. van Alsenoy, J. Comp. Chem. **9**, 620 (1988).

[18] A. Schäfer, H. Horn, and R. Ahlrichs, J. Chem. Phys. **97**, 2571 (1992).

[19] K. Eichkorn, O. Treutler, H. Öhm, M. Häser, and R. Ahlrichs, Chem. Phys. Lett. **242**, 652 (1995).

[20] A. Klamt and G. Schüürmann, J. Chem. Soc. Trans. 2 **5**, 799 (1993).

[21] A. E. Reed, R. B. Weinstock, and F. Weinhold, J. Chem. Phys. **83**, 735 (1985).

[22] S. Nose, J. Chem. Phys. **81**, 511 (1984).

[23] S. Nose, Mol. Phys. **52**, 255 (1984).

[24] W. G. Hoover, Phys. Rev. A **31**, 1695 (1985).

[25] M. Lundberg and P. E. M. Siegbahn, J. Phys. Chem. B **109**, 10513 (2005).

[26] K. Park and J-Z. Wang, Polyhedron **66**, 157 (2013).

[27] M. Winter, WebElements, http://www.webelements.com, Accessed December 31, 2013.